ACS Catalysis

Research Article

pubs.acs.org/acscatalysis

Dual Homogeneous and Heterogeneous Pathways in Photo- and Electrocatalytic Hydrogen Evolution with Nickel(II) Catalysts Bearing Tetradentate Macrocyclic Ligands

Lingjing Chen,[†] Gui Chen,[†] Chi-Fai Leung,[†] Shek-Man Yiu,[†] Chi-Chiu Ko,[†] Elodie Anxolabéhère-Mallart,[‡] Marc Robert,*[,‡] and Tai-Chu Lau*[,†]

[†]Institute of Molecular Functional Materials and Department of Biology and Chemistry, City University of Hong Kong, Tat Chee Avenue, Kowloon, Hong Kong SAR, China

[‡]Université Paris Diderot, Sorbonne Paris Cité, Laboratoire d'Electrochimie Moléculaire, Unité Mixte de Recherche Université−CNRS no. 7591, Bâtiment Lavoisier, 15 rue Jean de Baïf, 75205 Paris Cedex 13, France

Supporting Information

ABSTRACT: A series of nickel(II) complexes bearing tetradentate macrocyclic N_4, N_3S, and N_3P ligands were synthesized, and their photocatalytic activity toward proton reduction has been investigated by using $[Ir(dF(CF_3)ppy)_2(dmbpy)]PF_6$ ($dF(CF_3)ppy$ = 2-(2,4-difluorophenyl)-5-trifluoromethylpyridine and dmbpy = 4,4′-dimethyl-2,2′-dipyridyl) as the photosensitizer and triethylamine (TEA) as the sacrificial reductant. The complex $[Ni(L4)]^{2+}$ (L4 = 2,12-dimethyl-7-phenyl-3,11,17-triaza-7-phospha-bicyclo[11,3,1]heptadeca-1(17),13,15-triene), which bears a phosphorus donor atom, shows the highest efficiency with TON up to 5000 under optimized conditions, while the tetraaza macrocyclic nickel complexes $[Ni(L1)]^{2+}$ and $[Ni(L2)]^{2+}$ (L1 = 2,12-dimethyl-3,7,11,17-tetra-azabicyclo[11.3.1]heptadeca-1(17),2,11,13,15-pentaene; L2 = 2,12-dimethyl-3,7,11,17-tetra-azabicyclo[11.3.1]-heptadeca-1(17),13,15-triene) show lower photocatalytic activities. Transient UV−vis absorption and spectroelectrochemical experiments show that Ni(II) is reduced to Ni(I) under photocatalytic conditions. However, dynamic light scattering and mercury poisoning experiments suggest that the Ni(I) is further reduced to Ni(0) nanoparticles which are the real catalysts for H_2 production. Electrocatalytic proton reduction by $[Ni(L4)]^{2+}$ has also been investigated. In this case, the electrochemical behavior is consistent with a homogeneous pathway, and no Ni nanoparticles were observed on the electrode surface during the first few hours of electrolysis. However, on prolonged electrolysis for >17 h, nickel-based nanoparticles were observed on the electrode surface, which are active catalysts for H_2 production.

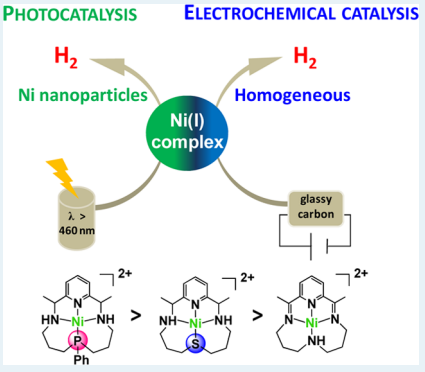

KEYWORDS: *hydrogen evolution, nickel catalyst, macrocyclic ligands, electrochemical catalysis, photocatalysis*

1. INTRODUCTION

In recent years, there has been an intense effort to develop artificial photosynthesis that can make use of solar energy to provide alternatives to fossil fuels. Light-induced splitting of water into O_2 and H_2 is an attractive strategy because molecular hydrogen is a clean and renewable fuel. Because the photosynthetic processes in nature are carried out in aqueous solutions and with metalloenzymes (homogeneous catalysts), considerable efforts have been put in by chemists to develop efficient molecular water reduction catalysts (WRCs) based on transition metal complexes for hydrogen production, including those of Pt,[1,2] Rh,[3,4] Mo,[5−7] Fe,[8−13] Co,[14−18] and Ni.[19−29] Another advantage of the molecular catalyst is to enable the identification of reactive intermediates and detailed kinetic study to provide some useful insights of catalytic mechanisms as well as the rational design of ligands for tailoring well-defined catalysts. However, the reaction conditions, such as aqueous solutions, strongly acidic or basic media, highly reducing potentials or intense light irradiation, may result in the transformation of the catalysts. Therefore, an important issue is to figure out whether the primary metal complex is the true homogeneous catalyst or just the precatalyst derived in situ by the transformations. This issue has been carefully discussed in water oxidation reaction by Finke,[30,31] Fukuzumi,[32,33] Lau,[34,35] Hill,[36] Beller,[37] and so on, but for electro- and photocatalytic hydrogen production, very few detailed studies have appeared.[38] We and others reported that the electrocatalytic hydrogen evolution by cobalt trisglyoximato-strapped clathrochelate complex,[39,40] cobalt pyridine oxime complex,[41] cobalt bisglyoximato complex,[42] and nickel bisglyoximato complex[43] in the presence of a strong acid (in aprotic solvent) results in electrodeposition of cobalt-based and nickel-based nanoparticles on the electrode surface. Roberts and co-workers also found that Ni−S films were electrodeposited onto glassy

Received: October 7, 2014
Revised: November 12, 2014
Published: December 1, 2014

carbon electrodes from $[Bu_4N][Ni(bdt)_2]$ (bdt = 1,2-benzenedithiolate) in acidic acetonitrile solutions, which are active toward electrocatalytic H_2 evolution.[44] For photocatalytic hydrogen production, a mercury poisoning test was usually carried out on non-noble metal complexes, such as cobaloxime,[45−47] cobalt aminopyridine,[48] nickel pyridinethiolate,[28] nickel-thiolate hexameric cluster[27] as well as nickel polyoxotungstate,[49] and the results were all negative with sustained activities.

In this paper, we have designed a series of nickel complexes based on the tetradentate macrocyclic ligand CR and its derivatives (CR = 2,12-dimethyl-3,7,11,17-tetra-azabicyclo[11.3.1]-heptadeca-1(17),2,11,13,15-pentaene; CR = L1 in Scheme 1) as proton reduction catalysts. The electrocatalytic proton reduction by $[Ni(CR)]^{2+}$ has previously been reported.[19] Although a number of nickel complexes bearing bidentate phosphine,[21−23] thiolate,[24−28] and amine[29] ligands have been reported for electrocatalytic and/or photocatalytic hydrogen production, we envisage that the use of macrocyclic ligands should stabilize the nickel catalysts and enhance their activity. For example, we and others recently reported that cobalt complexes bearing tetraazamacrocyclic ligands are efficient electrocatalysts and photocatalysts for proton reduction.[16,50−52] The ligands (L1−L6) contain N_4, N_3S, or N_3P donor atoms, and with different degrees of unsaturation. The effects of donor atom and ligand unsaturation on catalytic activity as well as the exact nature of the catalytic species have been investigated.

Scheme 1. Structure of Ligands

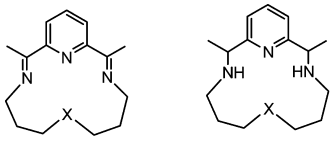

L1, X = NH
L3, X = P-Ph
L5, X = S

L2, X = NH
L4, X = P-Ph
L6, X = S

2. RESULTS AND DISCUSSION

2.1. Synthesis and Characterization of Nickel Catalysts. The Schiff-base nickel compounds $[Ni(L1)](ClO_4)_2$, $[Ni(L3)](ClO_4)_2$ and $[Ni(L5)_2(\mu\text{-}Cl)_2](ClO_4)_2$ were synthesized by template reaction of $NiCl_2{\cdot}6H_2O$ with 2,6-diacetylpyridine and the appropriate diamine in aqueous ethanol. On the other hand, $[Ni(L2)](ClO_4)_2$, $[Ni(L4)](ClO_4)_2$, and $[Ni(L6)](ClO_4)_2$ were obtained by direct reaction of the macrocyclic ligands with nickel(II) perchlorate. The structures of $[Ni(L3)](ClO_4)_2$, $[Ni(L4)](ClO_4)_2$, $[Ni(L5)_2(\mu\text{-}Cl)_2](ClO_4)_2$, and $[Ni(L6)](ClO_4)_2$ have been determined by X-ray crystallography (Figure 1, Table S1−S8). $[Ni(L3)]^{2+}$, $[Ni(L4)]^{2+}$ and $[Ni(L6)]^{2+}$ are four-coordinate with a distorted square-planar geometry. On the other hand, $[Ni(L5)_2(\mu\text{-}Cl)_2]^{2+}$ has a dimeric structure with two chloro bridges, and each nickel center adopts a distorted octahedral geometry with the macrocyclic ligand in a *cis* configuration. However, electrospray ionization mass spectrometry (ESI/MS, Figure S1) and cyclic voltammetry (CV, Figure S2) suggest that the complex is monomeric in CH_3CN solution. A conductivity experiment (see Experimental Section) showed that Cl^- should still be coordinated to the nickel center in solution. So the $[Ni(L5)_2(\mu\text{-}Cl)_2]^{2+}$ should exist as $[Ni(L5)Cl]^+$ in CH_3CN solution.

The cyclic voltammetry of the nickel complexes in CH_3CN has been investigated (Table 1 and Figure S3). The imine complexes, $[Ni(L1)]^{2+}$, $[Ni(L3)]^{2+}$ and $[Ni(L5)Cl]^+$ display

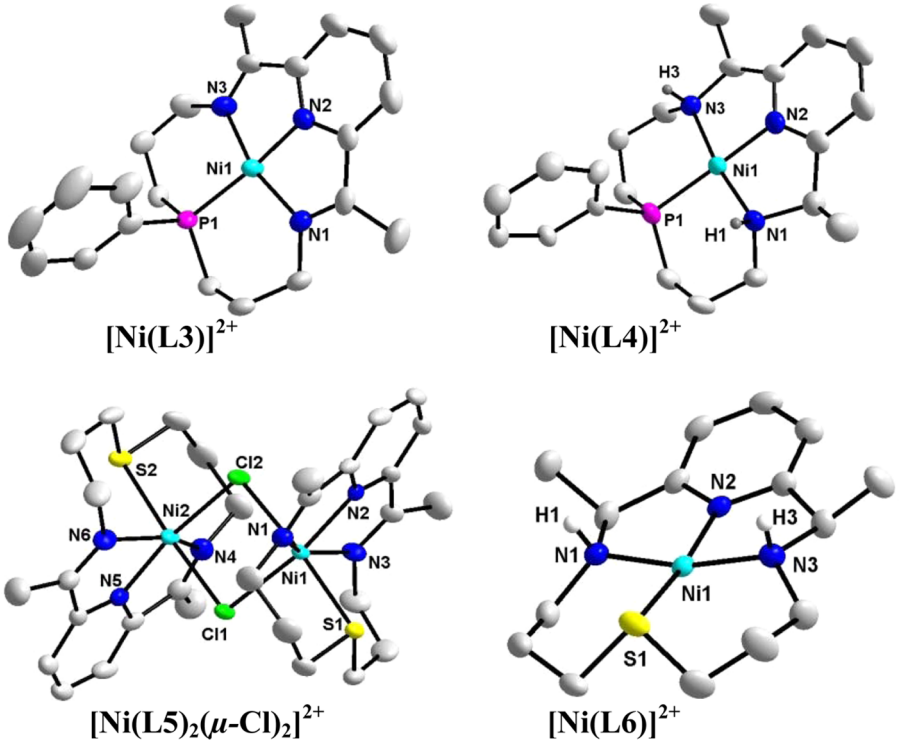

Figure 1. ORTEP drawings of $[Ni(L3)]^{2+}$, $[Ni(L4)]^{2+}$, $[Ni(L5)_2(\mu\text{-}Cl)_2]^{2+}$, and $[Ni(L6)]^{2+}$. Hydrogen atoms (except for N−H) are omitted for clarity. Thermal ellipsoids are drawn with 30% probability.

dx.doi.org/10.1021/cs501534h | ACS Catal. 2015, 5, 356−364

Table 1. Standard Redox Potentials of Ni Complexes Determined by CV (V vs SCE, 0.1 V/s)

nickel complexes	$Ni^{III/II}$ E^0 (ΔE_p,[a] mV)	ligand$^{0/\bullet-}$ E^0 (ΔE_p,[a] mV)	$Ni^{II/I}$ E^0 (ΔE_p,[a] mV)
$[Ni(L1)]^{2+}$	+1.38 (71)	−0.64 (69)	−1.20 (65)
$[Ni(L2)]^{2+}$	+1.23 (79)	—	−1.17 (71)
$[Ni(L3)]^{2+}$	+1.10[b]	−0.51 (65)	−1.02 (67)
$[Ni(L4)]^{2+}$	+1.31[b]	—	−0.98 (69)
$[Ni(L5)Cl]^{+}$	+1.23[b]	−0.67 (114)	−1.13 (71)
$[Ni(L6)]^{2+}$	+1.38 (71)	—	−0.88 (75)

[a]Separation between cathodic and anodic peak. [b]Anodic peak potential (irreversible wave).

two reversible one-electron reductions in CH_3CN. Based on the electrochemical work of Weighardt and co-workers on $[Ni(CR)]^{2+}$ (CR = L1),[53] the first reduction is most likely ligand-centered to produce $[Ni^{II}(L^{\bullet-})]^{+}$, while the second reduction is metal-centered to generate $[Ni^{I}(L^{\bullet-})]^{+}$. On the other hand, for the saturated nickel complexes $[Ni(L2)]^{2+}$, $[Ni(L4)]^{2+}$ and $[Ni(L6)]^{2+}$, only one reduction wave, corresponding to $[Ni(L)]^{2+/+}$, was observed. Notably the E^0 of the $Ni^{II/I}$ couple shifts to more positive value as a N donor atom in the macrocyclic ligand L is replaced by a softer donor atom P or S, consistent with stabilization of Ni^{I} by P or S through π-back bonding. The much more negative E^0 of $Ni^{II/I}$ for $[Ni(L5)Cl]^{+}$ than $[Ni(L6)]^{2+}$ is likely due to the presence of an additional chloro ligand in the former complex.

2.2. Photocatalytic Proton Reduction. The photocatalytic activity of the nickel-based catalysts toward proton reduction was evaluated by using $[Ir(dF(CF_3)ppy)_2(dmbpy)]PF_6$ ($[IrPS]^{+}$) as the photosensitizer and triethylamine (TEA) as the sacrificial reductant. Among the various solvent systems tested, 10% H_2O in THF is the best one, and TEA is a much better sacrificial reductant than triethanolamine (TEOA) (Table 2). The tetraaza macrocyclic complexes, $[Ni(L1)]^{2+}$ and $[Ni(L2)]^{2+}$, showed relatively low photocatalytic activity with turnover number (TON) of <300 after 24 h of irradiation at λ > 460 nm (Figure 2, left). Interesting, $Ni(ClO_4)_2$ is also active with a moderate TON of 524. On the other hand, nickel complexes with phosphorus or sulfur donor atoms gave much higher photocatalytic activity. For $[(Ni(L5)Cl]^{+}$ and $[Ni(L6)]^{2+}$, which contain a sulfur donor atom, the TON are 774 and 740, respectively, based on catalyst concentration. The nickel complexes $[Ni(L3)]^{2+}$ and $[Ni(L4)]^{2+}$, which contain a phosphorus donor atom, showed even higher TON of 960 and 1030, respectively. Using $[Ni(L4)]^{2+}$, which is the best catalyst, a TON of 4874 could be achieved after irradiation for 70 h under optimal conditions (Figure 2, right). These results demonstrate that the catalytic proton reduction activity of these nickel macrocyclic complexes is greatly affected by the donor atom. On the other hand, the catalytic activity is minimally affected by the degree of unsaturation on the ligand.

The higher catalytic activity of the phosphorus-containing complexes could be due to their lower reduction potentials (Table 1), which would result in faster reduction to Ni^{I}. Fluorescence quenching experiments showed that the luminescence of $[IrPS]^{+*}$ was quenched by TEA, and a rate constant of 1×10^9 M^{-1} s^{-1} was obtained from Stern−Volmer plot (Figure S4). The initial formation of [IrPS] was also demonstrated by transient UV−vis absorption spectroscopy and spectroelectrochemistry (Figure S5). [IrPS] is thermodynamically capable of reducing all the Ni^{II} complexes to Ni^{I}, because the E^0 for the $[IrPS]^{+}/[IrPS]$ couple is −1.36 V vs SCE in CH_3CN, as determined by CV (Figure S6). The formation of Ni^{I} upon photolysis in the presence of $[IrPS]^{+}$ and TEA is evidenced by the appearance of a brown species with λ_{max} at 427 nm upon photolysis, which is very similar to the spectrum of Ni^{I} obtained by spectroelectrochemical method (Figure S7). These results provide evidence for Ni^{I} as an intermediate, as least in the initial stages of photocatalysis.

We have also tried to use $[Ru(bpy)_3]^{2+}$, which has a milder PS with $[Ru(bpy)_3]^{2+/+}$ potential of −0.86 V vs NHE. However, using the $[RuPS]^{2+}$ with $[Ni(L4)]^{2+}$ as catalyst, a much lower amount of H_2 was observed (TON = 47, Figure S8). Also, in contrast to electrocatalysis, which was carried out under acidic conditions, the photocatalysis was carried out under basic conditions because the sacrificial donor TEA is a base. We have performed photocatalysis experiments under acidic conditions by adding CF_3CO_2H to TEA until pH = 4.0; however, a much lower TON of 148 was obtained (Figure S9).

Recent work by Fukuzumi[54] and Fu[55] show that zerovalent nickel nanoparticles are highly efficient for photocatalytic hydrogen evolution. In order to determine whether the Ni^{I} intermediate observed upon photocatalysis is the active species, or whether it is just a precatalyst that will decompose to Ni nanoparticles as the real catalyst, dynamic light scattering (DLS) experiments were performed using $[Ni(L4)]^{2+}$ as the catalyst. DLS analysis revealed the formation of nanoparticles of median size 250 nm after irradiation for 5 min, and the size increased to 350 nm after 2 h (Figure 3). However, the particles disappeared after 15 h of irradiation, and H_2 production stopped. Analysis of the reaction solution (after transferring to a clean flask, evaporating to dryness and redissolving in H_2SO_4/H_2O_2) by inductively coupled plasma atomic emission spectroscopy (ICP-AES) showed that only 10% of Ni was present. HNO_3 (2 M) was then added to the empty reaction

Table 2. Photocatalytic Hydrogen Production by $[Ni(L4)]^{2+}$ under Various Conditions

entry	$[Ni(L4)]^{2+}$ (mM)	$[IrPS]^{+}$ (mM)	sacrificial reductant	solvent	TON[a] (3 h)
1	0.1	1	0.6 M TEA	10% H_2O in CH_3CN	7
2	0.1	1	0.6 M TEA	10% H_2O in acetone	127
3	0.1	1	0.6 M TEA	10% H_2O in THF	369
4	0.1	1	0.6 M TEA	20% H_2O in THF	365
5	0.1	1	0.6 M TEA	5% H_2O in THF	220
6	0.1	1	0.6 M TEOA	10% H_2O in THF	10
7	0	1	0.6 M TEA	10% H_2O in THF	trace
8	0.1	0	0.6 M TEA	10% H_2O in THF	0
9	0.1	1	0 M TEA	10% H_2O in THF	0

[a]Defined as the number of catalytic cycles divided by the number of mole reactant.

dx.doi.org/10.1021/cs501534h | ACS Catal. 2015, 5, 356−364

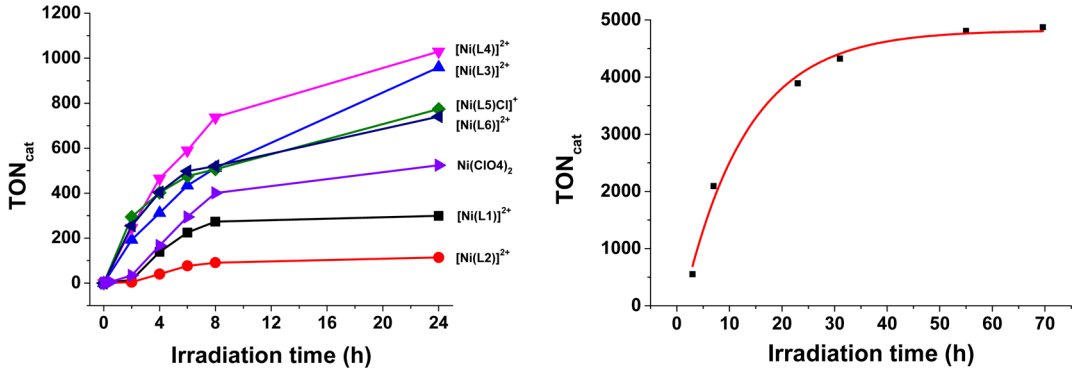

Figure 2. (left) Photocatalytic H_2 production by nickel complexes (0.1 mM) and $Ni(ClO_4)_2$ (0.1 mM) in 2.5 mL THF/H_2O (9:1, v/v) containing $[IrPS]^+$ (1 mM) and TEA (0.6 M) (λ > 460 nm, 24 h). (right) H_2 generation for $[Ni(L4)]^{2+}$ (0.01 mM), $[IrPS]^+$ (1 mM) and TEA (0.6 M) in 2.5 mL THF/H_2O (9:1, v/v) under irradiation for 70 h.

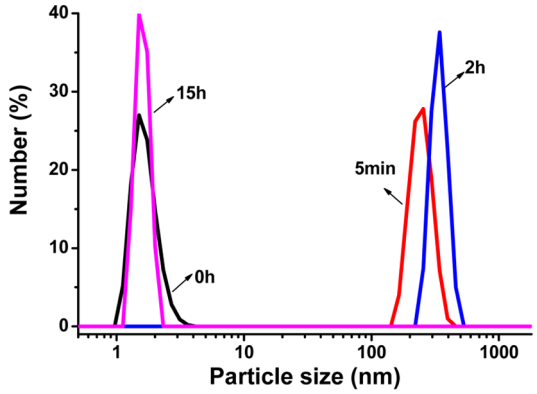

Figure 3. Particle distribution determined by DLS measurements during irradiation of a solution containing $[Ni(L4)]^{2+}$ (0.1 mM), $[IrPS]^+$ (1 mM), and TEA (0.6 M) in 2.5 mL of THF/H_2O (9:1, v/v).

vessel together with the stir bar, and after sonication, the solution was analyzed by ICP-AES, which showed the presence of 85% of the initial Ni. Nanoparticles were also observed for $[Ni(L1)]^{2+}$ (Figure S10) and $[Ni(L6)]^{2+}$ (Figure S11). These results demonstrate the formation of Ni-based nanoparticles during photocatalysis, which are probably the active catalysts. These particles gradually aggregate and eventually stick to the surface of the reaction vessel and the stir bar, resulting in loss of catalytic activity.

The particles formed during photocatalysis by $[Ni(L4)]^{2+}$ were also isolated and characterized by scanning electron microscopy (SEM) and energy-dispersive X-ray spectroscopy (EDX). The SEM image shows that the solid consists of aggregates of submicron particles, and EDX reveals that the solid contains only Ni, O, and P (Figure 4). These results provide further evidence that nickel-based nanoparticles are formed during photocatalysis.

Mercury poisoning experiments have also been performed. A vigorously stirred solution of 0.1 mM $[Ni(L4)]^{2+}$, 1 mM $[IrPS]^+$, and 0.6 M TEA containing 5 μL of Hg was irradiated (Figure 5). H_2 evolution was found to be significantly blocked,

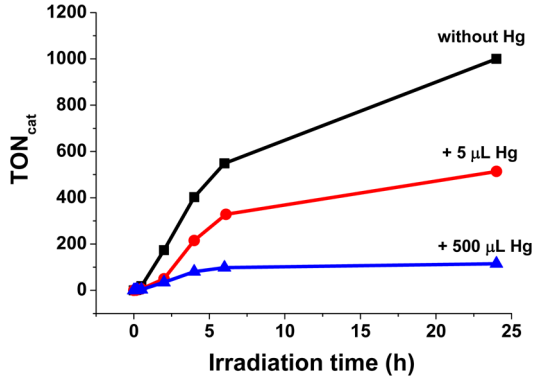

Figure 5. Plot of H_2 generation from a system consisting in $[Ni(L4)]^{2+}$ (0.1 mM), $[IrPS]^+$ (1 mM), and TEA (0.6 M) in 2.5 mL of THF/H_2O (9:1, v/v) under irradiation for 24 h in the absence and presence of mercury.

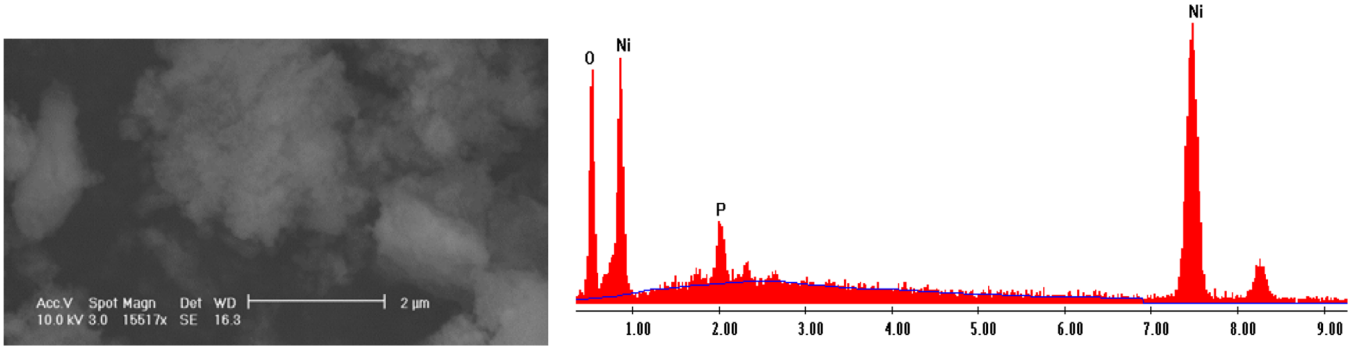

Figure 4. SEM image (left) and EDX spectrum (right) of particles formed by irradiation of 25 mL of THF/H_2O (9:1, v/v) solution containing $[Ni(L4)]^{2+}$ (1 mM), $[IrPS]^+$ (1 mM), and TEA (0.6 M) for 10 h.

dx.doi.org/10.1021/cs501534h | ACS Catal. 2015, 5, 356−364

and the total amount of H_2 was reduced by 50% after 24 h. In the presence 500 μL of Hg, the yield was further reduced to 12%. Ni(0) is known to form an amalgam with mercury,[38] so the observation that the catalytic system is deactivated in the presence of mercury suggests that nickel(0) nanoparticles are formed during irradiation, which are the active catalytic species.

The relative rates of decomposition of the Ni(II) complexes to Ni(0) nanoparticles during photocatalysis were also investigated for $[Ni(L1)]^{2+}$, $[Ni(L4)]^{2+}$, and $[Ni(L6)]^{2+}$. Aliquots were withdrawn at various time intervals and then centrifuged for 10 min at 13 000 rpm. The supernatant solution was then analyzed by ICP-AES. The Ni content analyzed in this way would reflect the amount of nickel complexes still present in the solution at various intervals. From Figure 6 it can be seen

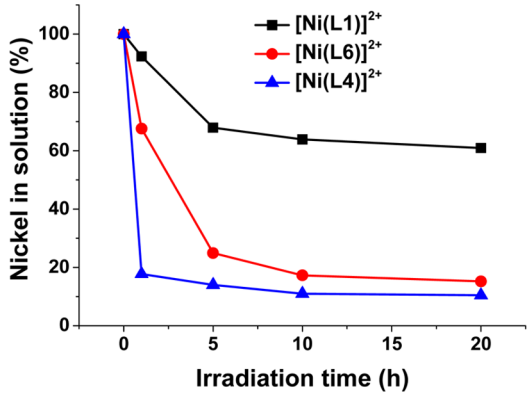

Figure 6. Percentage of nickel in solution as a function of time during photocatalytic H_2 production from 2.5 mL THF/H_2O (9:1, v/v) solution containing nickel catalysts (0.1 mM), $[IrPS]^+$ (1 mM), and TEA (0.6 M).

that the degradation rates of the nickel catalysts follow the same order as their photocatalysis rates, that is, $[Ni(L4)]^{2+}$ > $[Ni(L6)]^{2+}$ > $[Ni(L1)]^{2+}$. For $[Ni(L4)]^{2+}$, only 20% of the initial complex remains in the solution after irradiation of 1 h, while 68% and 92% of $[Ni(L6)]^{2+}$ and $[Ni(L1)]^{2+}$, respectively, are still present (Figure 6). At longer times, most of the $[Ni(L4)]^{2+}$ and $[Ni(L6)]^{2+}$ are transformed into particles, whereas more than 60% of the initial $[Ni(L1)]^{2+}$ complex is still present.

On the basis of the above results, we conclude that in photocatalytic proton reduction, the Ni(II) complexes are first reduced to Ni(I) complexes upon irradiation in the presence of $[IrPS]^+$ and TEA, which are then further reduced to form Ni(0) nanoparticles as the real catalyst for H_2 production. H_2 production stops when the nanaparticles eventally aggregate to micron-size particles and stick to the surface of the reaction vessel and stir bar. Although the Ni(II) complexes function only as precatalysts, the macrocyclic ligands play an important role in the formation of the catalytically active Ni nanoparticles, as evidenced by the observation that simple Ni(II) salts such as $Ni(ClO_4)_2$ is not a very efficient catalyst (Figure 2). On the other hand, Ni(II) complexes with P or S donor atom in the macrocyclic ligand are much more efficient precatalysts than those with only N donor atoms, because they have less negative Ni^{II}/Ni^{I} redox potentials and are therefore more easily reduced to Ni(I) by [IrPS] and then to Ni nanoparticles.

2.3. Electrocatalytic Proton Reduction. Electrocatalytic H_2 production activity of the best photocatalyst, $[Ni(L4)]^{2+}$, was also investigated. Perchloric ($HClO_4$) or trifluoroacetic acid (TFA) was used as the proton source in acetonitrile. Addition of the acid triggers a catalytic wave at a potential close to the Ni^{II}/Ni^{I} couple, as shown in Figure 7. Catalysis is stronger with

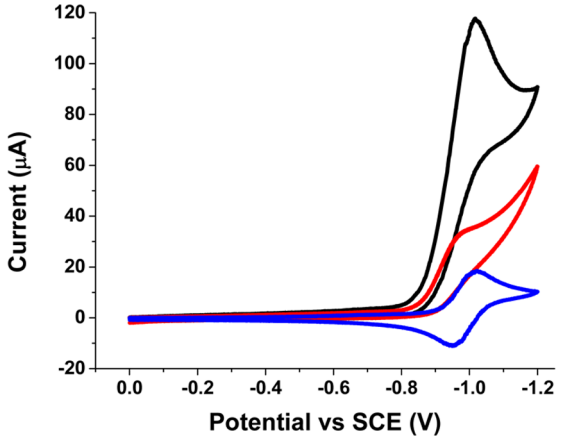

Figure 7. CV of $[Ni(L4)]^{2+}$ (1 mM) in the absence (blue) and presence of $HClO_4$ (10 mM, black) and TFA (10 mM, red). Scan rate = 0.1 V/s.

the stronger acid ($HClO_4$), leading in both cases to hydrogen formation. Repeated controlled-potential electrolysis performed at −0.95 V vs SCE with 1 mM $[Ni(L4)]^{2+}$ in CH_3CN using $HClO_4$ as the proton source produced hydrogen with 75 to 85% faradaic yields (see Figure S13 for a typical example). From the average electrolysis current, estimation of the first-order catalytic rate constant leads to a value of 220 s^{-1} (see Scheme S2 and Figure S13 for a detailed explanation). Benchmarking evaluation of molecular catalysts regarding H_2 evolution has recently been proposed based on log TOF vs overpotential performance comparison.[56] With a turnover frequency of 220 per second at an overpotential $\eta = E^0(H^+/H_2) - E_{electrolysis} = +0.12^{57} - (-0.95) = 1.07$ V, $[Ni(L4)]^{2+}$ appears as an efficient catalyst (see Figure 4 in ref 56 for a comparison with the most active molecular metal based H_2-catalysts so far reported in the literature).

On the basis of photocatalytic studies and previous electrochemical studies,[39−44] investigation was carried out to check whether there is any electrodeposition on the electrode surface during H_2 production. First, CV of $[Ni(L4)]^{2+}$ (0.1 to 1 mM) with 10 mM $HClO_4$ (Figure S12) in 0.1 M $^nBu_4NPF_6$ in CH_3CN showed an increase in peak current with an increase in nickel concentration, which is coherent with homogeneous catalysis. Second, when continuous linear sweep voltammetry was performed for 5 times in 0.1 M $^nBu_4NPF_6$ CH_3CN solution containing 1 mM $[Ni(L4)]^{2+}$ and 10 mM $HClO_4$, the intensity of the catalytic currents were almost the same (Figure 8). After rinsing the electrode and then performing a linear scan in fresh 0.1 M $^nBu_4NPF_6$ CH_3CN solution containing 10 mM $HClO_4$ without catalyst, no catalytic current was observed (Figure 8). Controlled-potential electrolysis experiments with glassy carbon electrode (3 mm diameter) were also further analyzed. After electrolyzing at −0.95 V for 4 h (Figure S13), SEM analysis of the electrode surface showed that no nickel film or nanoparticles were deposited on the surface (Figure S14). EDX showed that there was only carbon on the electrode surface (Figure S15). In addition, UV−vis spectroscopy showed that 98.5% of $[Ni(L4)]^{2+}$ was still in the solution (Figure S16).

dx.doi.org/10.1021/cs501534h | ACS Catal. 2015, 5, 356−364

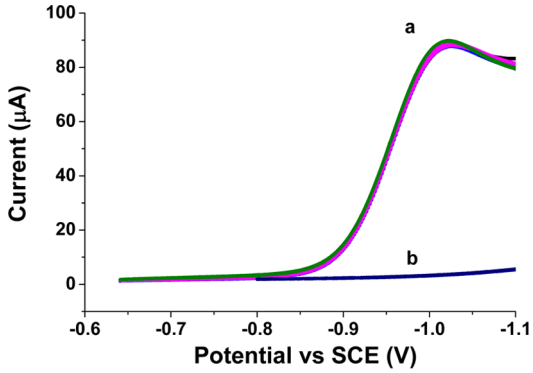

Figure 8. (a) Continuous linear scan (5 times) of a solution containing 1 mM $[Ni(L4)]^{2+}$ and 10 mM $HClO_4$ in 0.1 M $^nBu_4NPF_6$ in CH_3CN. (b) Voltammogram using the electrode scanned 5 times in (a), in a fresh solution containing 10 mM $HClO_4$ + 0.1 M $^nBu_4NPF_6$ in CH_3CN without catalyst. Scan rate = 0.1 V/s.

However, on prolonging the electrolysis time to 17.6 h (H_2 yield 74%), particles from 100 to 300 nm in size were clearly observed on the electrode surface by SEM (Figure 9), and EDX

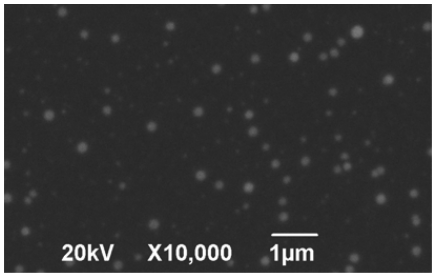

Figure 9. SEM image of the electrode surface after electrolysis of a solution containing $[Ni(L4)]^{2+}$ in 10 mM $HClO_4$ for 17.6 h at −0.95 V vs SCE using glassy carbon electrode (3 mm diameter) as working electrode.

analysis showed the presence of Ni, P, and O (Figure S17). When the electrolyte was removed under Ar atmosphere, followed by addition of 10 mL of degassed phosphate buffer solution (0.1 M, pH 7), and then linear sweep scan was performed, an intense cathodic current could be observed (Figure 10). Note that the electrode was almost inactive without catalytic current after exposure to the air, presumably because the nickel was oxidized to nickel oxide (Figure 10).

These results show that during the first few hours of catalysis, the mechanism is homogeneous, but on prolonged electrolysis, the mechanism switches to heterogeneous, with Ni nanoparticles acting as highly active catalysts.

3. CONCLUSIONS

In conclusion, we have demonstrated an interesting case of dual homogeneous and heterogeneous pathways in photo- and electrocatalytic proton reduction by macrocyclic nickel(II) complexes. The photocatalysis follows a heterogeneous pathway, while the electrochemical catalysis follows a homogeneous pathway at short electrolysis time; however, it switches to a heterogeneous pathway on prolonged electrolysis. In photocatalytic proton reduction using a Ir(III) cyclometalated complex as photosensitizer and triethylamine as sacrificial reductant, the Ni(II) complex is first reduced to Ni(I) complex which undergoes further reduction and demetalation and to

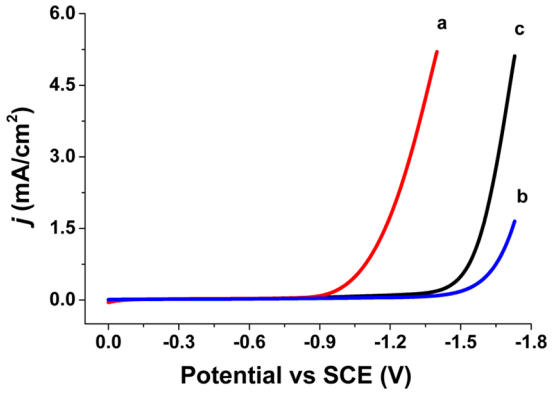

Figure 10. Linear sweep voltammetry (LSV) in phosphate buffer at pH 7 (0.1 M, ν = 0.1 V/s) at a glassy carbon electrode. (a) Modified electrode (see text), rinsed with CH_3CN and dried under Ar atmosphere. (b) Modified electrode exposed to air prior to LSV. (c) Freshly polished, unmodified electrode.

generate Ni nanoparticles as the real catalyst for proton reduction. Ni(II) complexes with π-donor atoms such as P or S have less negative $Ni^{II/I}$ redox potentials; hence they are more readily reduced to Ni(I) and they are more efficient catalysts than Ni(II) complexes with only N-donor atoms or simple Ni(II) salts. On the other hand, in electrocatalytic proton reduction, the molecular Ni(II) complexes are active catalysts at short electrolysis time, but at longer time Ni(0), particles become the real catalyst.

In photocatalysis, the reaction medium contains excess triethylamine and is therefore basic, whereas in electrochemical catalysis, the reaction medium is acidic. Presumably, the Ni(I) species is much less stable in basic than in acidic medium, and hence, Ni nanoparticles are readily produced in photocatalysis. It is also possible that the Ni(I) species is light sensitive and gradually undergoes demetalation upon irradiation.

EXPERIMENTAL SECTION

Materials. 2,6-Diacetylpyridine (Sigma-Aldrich, 99%), 3,3′-diaminodipropylamine (Sigma-Aldrich, 98%), bis(2-cyanoethyl)phenylphosphine (Strem, 97%), 3,3-thiodipropionnitrile (TCI, 98%), sodium borohydride (Acros, 99%), lithium aluminum hydride (Acros, 95%), formic acid (Acros, 98%), formaldehyde (Acros, 37%), nickel(II) chloride hexahydrate (Sigma-Aldrich, 98%), nickel(II) perchlorate hexahydrate (Strem, 99%), nickel(II) nitrate hexahydrate (Strem, 99.999%), lithium perchlorate (Acros, 99%), triethanolamine (Acros, 99%), triethylamine (Acros, 99.7%), tetrakis(triphenylphosphine)palladium(0) (Acros, 99%), 4,4′-dimethyl-2,2′-dipyridyl (Sigma-Aldrich, 99%), 2-chloro-5-(trifluoromethyl)pyridine (Acros, 98%), 2,4-difluorophenylboronic acid (Acros, 98%), iridium(III) chloride hydrate (Sigma-Aldrich, reagent grade), trifluoroacetic acid (Sigma-Aldrich, 99%), acetic acid (Sigma-Aldrich, 99.8%), 4-aminobenzonitrile (Acros, 98%), and boric acid (Acros, 99%) were used as received without further purification. $^nBu_4NPF_6$ was recrystallized three times from ethanol and dried at 120 °C overnight. $[Ni(L1)](ClO_4)_2$,[58,59] $[Ni(L2)](ClO_4)_2$,[59] bis(3-aminopropyl)-phenylphosphine,[60] 4-thia-1,7-heptanediamine,[60] and $[Ir(dF(CF_3)ppy)_2(dmbpy)]PF_6$[61] were synthesized according to literature procedures.

Synthesis and Characterization. *$[Ni(L3)](ClO_4)_2$.* $[Ni(L3)](ClO_4)_2$ was prepared according to the literature with

dx.doi.org/10.1021/cs501534h | ACS Catal. 2015, 5, 356−364

some modifications.[59,62,63] 2,6-Diacetylpyridine (1.63 g, 0.01 mol), $NiCl_2·6H_2O$ (2.38 g, 0.01 mol), and bis(3-aminopropyl)-phenylphosphine (2.24 g, 0.01 mol) were dissolved in 15 mL of ethanol and 15 mL of water. After stirring for 5 min, 0.5 mL of acetic acid was added under argon, and the solution was further stirred at 80 °C for 6 h. After removing half of the solvent under reduced pressure, the solution was filtered. Lithium perchlorate (4.28 g, 0.04 mol) was added, and the solution was stirred at room temperature for 1 h. The resulting precipitate was collected on a sintered glass funnel and washed with ethanol followed by diethyl ether. The product was recrystallized by slow diffusion of diethyl ether into a concentrated acetonitrile solution of the compound. Yield: 4.63 g (76%). ESI/MS: m/z = 508 ($[Ni(L3)](ClO_4)^+$. Anal. Calcd for $C_{21}H_{26}Cl_2N_3NiO_8P·0.5CH_3CN$: C, 41.97; H, 4.40; N, 7.79. Found: C, 41.56; H, 4.54; N, 8.05.

L4. L4 was prepared according a reported procedure with some modifications.[59] 2,6-Diacetylpyridine (1.63 g, 0.01 mol), $NiCl_2·6H_2O$ (2.38 g, 0.01 mol), and bis(3-aminopropyl)-phenylphosphine (2.24 g, 0.01 mol) were dissolved in 15 mL of ethanol and 15 mL of water. Acetic acid (0.5 mL) was then added under argon, and the solution was stirred at 80 °C for 6 h. The resulting solution was cooled to room temperature and then put in an ice bath. Sodium borohydride (1.50 g, 0.04 mol) was added in three portions over 30 min. The reaction mixture was then stirred overnight under argon and then heated at 80 °C for 2 h. Ethanol was removed by evaporation, and sodium cyanide (4.0 g, 0.082 mol) was added. After heating at 80 °C for 2 h, the reaction mixture was cooled. The solution was adjusted to pH > 12 with 10% NaOH solution and then extracted with dichloromethane (3 × 50 mL). The combined extracts were evaporated to give ligand L4 which was stored under argon. The ligand was used for next step without any purification. Yield: 2.24 g (63%).

$[Ni(L4)](ClO_4)_2$. L4 (0.71 g, 0.002 mol) was dissolved in 10 mL ethanol, and $Ni(ClO_4)_2·6H_2O$ (0.75 g, 0.002 mol) was added. After the mixture was stirred at room temperature for 30 min, the orange yellow solid was collected on a fritted glass funnel, washed with ethanol and then diethyl ether. The product was recrystallized by slow diffusion of diethyl ether into a concentrated acetonitrile solution of the compound. Yield: 3.37 g (55%). ESI/MS: m/z = 512 ($[Ni(L4)]ClO_4)^+$. ^{1}H NMR (400 MHz, DMSO): 8.52 (d, J = 7.2 Hz, 2H), 8.27 (t, J = 8.0 Hz, 1H), 7.56−7.67 (m, 5H), 4.67−4.71 (m, 2H), 4.26−4.30 (m, 2H), 2.60−2.80 (m, 4H), 1.86−2.02 (m, 4H), 1.58 (d, J = 7.2, 6H), 1.00−1.13 (m, 2H). Anal. Calcd for $C_{21}H_{30}Cl_2N_3NiO_8P·CH_3CN$: C, 42.23; H, 5.09; N, 8.57. Found: C, 42.20; H, 5.08; N, 8.57.

$[(Ni(L5)_2(\mu\text{-}Cl)_2](ClO_4)_2$. This was prepared using the similar method as $[Ni(L3)](ClO_4)_2$. Yield: 56%. ESI/MS: m/z = 368 ($[Ni(L5)Cl])^+$, 432 ($[Ni(L5)]ClO_4)^+$. Anal. Calcd for $C_{30}H_{42}Cl_4N_6Ni_2O_8S_2$: C, 38.41; H, 4.51; N, 8.96. Found: C, 38.52; H, 4.41; N, 9.07.

$[Ni(L6)](ClO_4)_2$. The preparation of $[Ni(L6)](ClO_4)_2$ was similar to that of $[Ni(L4)](ClO_4)_2$ except that 4-thia-1,7-heptanediamine was used instead of bis(3-aminopropyl)-phenylphosphine. Yield: 43%. ESI/MS: m/z = 436 ($[Ni(L6)]-ClO_4)^+$. Anal. Calcd for $C_{15}H_{25}Cl_2N_3NiO_8S$: C, 33.55; H, 4.69; N, 7.82 . Found: C, 33.70; H, 4.50; N, 7.83.

Instrumentation. Electrospray ionization mass spectra (ESI/MS) were obtained on a PE SCIEX API 150 mass spectrometer. The analytic solution was continuously infused with a syringe pump at a constant flow rate into the pneumatically assisted electrospray probe with nitrogen as the nebulizing gas. ^{1}H NMR spectra were recorded on a Bruker 400 MHz spectrometer, and the chemical shift is expressed in ppm. Elemental analyses were done on an Elementar Vario EL analyzer. X-ray crystallography measurements were collected on an Oxford Gemini Ultra diffractometer with a monochromated Cu Kα radiation (λ = 1.54178 Å). DLS measurements were performed by using a Zetasizer Nano ZS instrument (Malvern Instruments Ltd., U.S.A.), which can detect particle sizes ranging from 0.6−6000 nm. The light source was a HeNe gas laser (4 mW, λ = 632.8 nm). Data were obtained by using a scattering angle of 175° at 23 °C. SEM and EDX were performed by using a Philips XL30 environmental scanning electron microscope at an accelerating voltage of 10 and 25 kV, respectively. Metal analysis was done on a PE2100 ICP-AES.

Photocatalytic Studies of Hydrogen Evolution. Photocatalytic hydrogen evolution was conducted in a glass tube (1.8 cm × 18 cm, total volume of 28 mL) sealed with a rubber septum. The light source was a RGB tricolor LED light strip with 9 modules purchased from www.creativelightings.com. Each LED module consists of three light sources (blue, green, and red), and the final light color is white (>460 nm). The gas phase in the head space was analyzed by GC/TCD (Galaxie 430) fitted with a Chrompack 5 Å molecular sieve column (30 m × 0.32 mm × 1.5 μm) with Ar as carrying gas. Hydrogen calibration curve was obtained by filling pure hydrogen gas to a tube with a graduated gastight syringe.

Fluorescence Quenching. The quenching experiments were performed by addition of certain amounts of TEA with a gastight syringe into 2.5 mL of aqueous THF solution (10% H_2O) in a quartz cuvette sealed with a septum at room temperature. The concentration of $[IrPS]^+$ was fixed at 0.04 mM. The solution was degassed under Ar for 30 min. Steady-state luminescence spectra were then collected on a SPEX FluoroLog 3-TCSPC spectrofluorometer. The relative emission intensity or lifetime of the characteristic emission of the iridium complex in the presence of different concentrations of TEA was used to calculate the quenching rate constant (k_q) with Stern−Volmer equation.[64]

$$I_0/I \text{ or } \tau_0/\tau = 1 + k_q\tau_0[Q]$$

where I_0 and I are the integrated MLCT emission intensity in the absence and presence of TEA, τ_0 and τ are the excited state lifetime in the absence and presence of TEA, k_q is the quenching rate constant, and $[Q]$ is the concentration of TEA.

Transient Absorption. Transient absorption spectra at room temperature were recorded using the spectral mode on an Edinburgh Instruments LP920-KS spectrometer equipped with an ICCD detector. The excitation source for the transient absorption measurement was the third harmonic output (355 nm; 6−8 ns fwhm pulse width) of a Spectra-Physics Quanta-Ray Q-switched LAB-150 pulsed Nd:YAG laser (10 Hz). Samples were deaerated for 30 min with argon before measurements.

Spectroelectrochemical Studies. Spectroelectrochemical measurements were carried out in a quartz cell with an optical path length of 1 cm. A carbon cloth strip (N0S1005 from Ce Tech), a platinum net, and a nonaqueous $Ag/AgNO_3$ were used as working electrode, counter electrode, and reference electrode, respectively. The sample solutions were deaerated with acetonitrile-saturated argon. The spectra were recorded on an Agilent 8453 UV−vis spectrophotometer during electrolysis on a CHI 660C instrument.

Electrochemical Studies. Cyclic voltammetry was performed with a CHI 660C instrument or a Metrohm AUTOLAB instrument. A glassy carbon (3 mm diameter) was used as working electrode, a platinum net as counter electrode, Ag/$AgNO_3$ or saturated calomel electrode (SCE) as reference electrode. The solution was purged with acetonitrile-saturated argon. Unless otherwise noted, all potentials in this study were adjusted to SCE using ferrocenium/ferrocene ($Fc^{+/0}$) couple (0.38 V vs SCE in CH_3CN)[65] as internal standard.

Bulk electrolysis was performed with a Princeton Applied Research Potentiostat (PARSTAT 2273) with a carbon crucible with a copper wire as working electrode (Scheme S1)[66] or a CHI 660C instrument with a glassy carbon (3 mm diameter) as working electrode. The reference electrode was an aqueous SCE electrode, and the counter electrode was a platinum net separated from the electrolyte by a bridge containing 0.4 M $Et_4N(CH_3CO_2)$ and 0.1 M $^nBu_4NPF_6$ in CH_3CN solution. The volume of the electrolysis solution was 9 mL and the solution was purged with Ar for 30 min prior to electrolysis. The reference electrode was directly immerged in the solution (without separated bridge) to minimize Ohmic drop. The gas phase in the head space was analyzed by GC/TCD (Galaxie 430) fitted with a Chrompack 5 Å molecular sieve column (30 m × 0.32 mm × 1.5 μm) with Ar as carrying gas. Hydrogen calibration curve was obtained by filling pure hydrogen gas to a tube with a graduated gastight syringe.

Metal Analysis with ICP-AES. Twenty-five milliliters of THF/H_2O (9:1, v/v) containing nickel complexes (0.1 mM), $[IrPS]^+$ (1 mM) and TEA (0.6 M) in a 100 mL Schlenk tube sealed with a rubber septum was degassed with Ar for 30 min and then irradiated. At regular intervals, 2 mL of the mixture was sampled by a syringe and centrifuged for 10 min at 13 000 rpm. One milliliter of the upper layer clear solution was evaporated to dryness, and then the residue was dissolved in H_2SO_4/H_2O_2 and analyzed by ICP-AES.

Conductivity Experiment. The conductivity of 1 mM $^nBu_4NPF_6$ in CH_3CN was found to be 152 μS/cm. The conductivity of 1 mM $[Ni_2(L5)_2(\mu\text{-}Cl)_2](ClO_4)_2$ was 292 μS/cm, which is about twice that of $^nBu_4NPF_6$, and as expected if no Cl- dissocation occurs in CH_3CN solution.

■ ASSOCIATED CONTENT

Supporting Information

The following files are available free of charge on the ACS Publications website at DOI: 10.1021/cs501534h.

ESI/MS spectra, electrochemical data, and other selected data (PDF)
Crystallographic data file 1 (CIF)
Crystallographic data file 2 (CIF)
Crystallographic data file 3 (CIF)
Crystallographic data file 4 (CIF)
checkCIF/PLATON report 1 (PDF)
checkCIF/PLATON report 2 (PDF)
checkCIF/PLATON report 3 (PDF)
checkCIF/PLATON report 4 (PDF)

■ AUTHOR INFORMATION

Corresponding Authors

*E-mail: robert@univ-paris-diderot.fr.
*E-mail: bhtclau@cityu.edu.hk.

Notes

The authors declare no competing financial interest.

■ ACKNOWLEDGMENTS

The work described in this paper was supported by Hong Kong University Grants Committee Area of Excellence Scheme (AoE/P-03-08), the Shenzhen Science and Technology Research Grant (JCYJ20120613115247045) and France/Hong Kong Joint Research Scheme (F-CityU105/13 and PHC Procore grant 24954SE).

■ REFERENCES

(1) Yamauchi, K.; Masaoka, S.; Sakai, K. *J. Am. Chem. Soc.* **2009**, *131*, 8404−8406.
(2) Ozawa, H.; Sakai, K. *Chem. Commun.* **2011**, *47*, 2227−2242.
(3) Cline, E. D.; Adamson, S. E.; Bernhard, S. *Inorg. Chem.* **2008**, *47*, 10378−10388.
(4) Xie, J.; Li, C.; Zhou, Q.; Wang, W.; Hou, Y.; Zhang, B.; Wang, X. *Inorg. Chem.* **2012**, *51*, 6376−6384.
(5) Appel, A. M.; DuBois, D. L.; DuBois, M. R. *J. Am. Chem. Soc.* **2005**, *127*, 12717−12726.
(6) Karunadasa, H. I.; Chang, C. J.; Long, J. R. *Nature* **2010**, *464*, 1329−1333.
(7) Karunadasa, H. I.; Montalvo, E.; Sun, Y. J.; Majda, M.; Long, J. R.; Chang, C. J. *Science* **2012**, *335*, 698−702.
(8) Bhugun, I.; Lexa, D.; Savéant, J.-M. *J. Am. Chem. Soc.* **1996**, *118*, 3982−3983.
(9) Ott, S.; Kritikos, M.; Akermark, B.; Sun, L. C.; Lomoth, R. *Angew. Chem., Int. Ed.* **2004**, *43*, 1006−1009.
(10) Gärtner, F.; Sundararaju, B.; Surkus, A.-E.; Boddien, A.; Loges, B.; Junge, H.; Dixneuf, P. H.; Beller, M. *Angew. Chem., Int. Ed.* **2009**, *48*, 9962−9965.
(11) Kaur-Ghumaan, S.; Schwartz, L.; Lomoth, R.; Stein, M.; Ott, S. *Angew. Chem., Int. Ed.* **2010**, *49*, 8033−8036.
(12) Wang, F.; Liang, W.-J.; Jian, J.-X.; Li, C.-B.; Chen, B.; Tung, C.-H.; Wu, L.-Z. *Angew. Chem., Int. Ed.* **2013**, *52*, 8134−8138.
(13) Yu, T.; Zeng, Y.; Chen, J.; Li, Y.-Y.; Yang, G.; Li, Y. *Angew. Chem., Int. Ed.* **2013**, *52*, 5631−5635.
(14) Hu, X. L.; Brunschwig, B. S.; Peters, J. C. *J. Am. Chem. Soc.* **2007**, *129*, 8988−8998.
(15) Lazarides, T.; McCormick, T.; Du, P.; Luo, G.; Lindley, B.; Eisenberg, R. *J. Am. Chem. Soc.* **2009**, *131*, 9192−9194.
(16) Leung, C.-F.; Chen, Y.-Z.; Yu, H.-Q.; Yiu, S.-M.; Ko, C.-C.; Lau, T.-C. *Int. J. Hydrogen Energy* **2011**, *36*, 11640−11645.
(17) McNamara, W. R.; Han, Z.; Alperin, P. J.; Brennessel, W. W.; Holland, P. L.; Eisenberg, R. *J. Am. Chem. Soc.* **2011**, *133*, 15368−15371.
(18) Singh, W. M.; Baine, T.; Kudo, S.; Tian, S. L.; Ma, X. A. N.; Zhou, H. Y.; DeYonker, N. J.; Pham, T. C.; Bollinger, J. C.; Baker, D. L.; Yan, B.; Webster, C. E.; Zhao, X. *Angew. Chem., Int. Ed.* **2012**, *51*, 5941−5944.
(19) Efros, L. L.; Thorp, H. H.; Brudvig, G. W.; Crabtree, R. H. *Inorg. Chem.* **1992**, *31*, 1722−1724.
(20) McLaughlin, M. P.; McCormick, T. M.; Eisenberg, R.; Holland, P. L. *Chem. Commun.* **2011**, *47*, 7989−7991.
(21) Helm, M. L.; Stewart, M. P.; Bullock, R. M.; DuBois, M. R.; DuBois, D. L. *Science* **2011**, *333*, 863−866.
(22) Stewart, M. P.; Ho, M.-H.; Wiese, S.; Lindstrom, M. L.; Thogerson, C. E.; Raugei, S.; Bullock, R. M.; Helm, M. L. *J. Am. Chem. Soc.* **2013**, *135*, 6033−6046.
(23) Gross, M. A.; Reynal, A.; Durrant, J. R.; Reisner, E. *J. Am. Chem. Soc.* **2013**, *136*, 356−366.
(24) Zhang, W.; Hong, J.; Zheng, J.; Huang, Z.; Zhou, J.; Xu, R. *J. Am. Chem. Soc.* **2011**, *133*, 20680−20683.
(25) Han, J.; Zhang, W.; Zhou, T.; Wang, X.; Xu, R. *RSC Adv.* **2012**, *2*, 8293−8296.
(26) Cui, H.-h.; Wang, J.-y.; Hu, M.-q.; Ma, C.-b.; Wen, H.-m.; Song, X.-w.; Chen, C.-n. *Dalton Trans.* **2013**, *42*, 8684−8691.
(27) Kagalwala, H. N.; Gottlieb, E.; Li, G.; Li, T.; Jin, R.; Bernhard, S. *Inorg. Chem.* **2013**, *52*, 9094−9101.

(28) Han, Z.; Shen, L.; Brennessel, W. W.; Holland, P. L.; Eisenberg, R. *J. Am. Chem. Soc.* **2013**, *135*, 14659−14669.
(29) Dong, J.; Wang, M.; Li, X.; Chen, L.; He, Y.; Sun, L. *ChemSusChem* **2012**, *5*, 2133−2138.
(30) Stracke, J. J.; Finke, R. G. *J. Am. Chem. Soc.* **2011**, *133*, 14872−14875.
(31) Stracke, J. J.; Finke, R. G. *ACS Catal.* **2014**, *4*, 909−933.
(32) Hong, D.; Jung, J.; Park, J.; Yamada, Y.; Suenobu, T.; Lee, Y.-M.; Nam, W.; Fukuzumi, S. *Energy Environ. Sci.* **2012**, *5*, 7606−7616.
(33) Hong, D.; Mandal, S.; Yamada, Y.; Lee, Y.-M.; Nam, W.; Llobet, A.; Fukuzumi, S. *Inorg. Chem.* **2013**, *52*, 9522−9531.
(34) Chen, G.; Chen, L.; Ng, S.-M.; Man, W.-L.; Lau, T.-C. *Angew. Chem., Int. Ed.* **2013**, *52*, 1789−1791.
(35) Chen, G.; Chen, L.; Ng, S.-M.; Lau, T.-C. *ChemSusChem* **2014**, *7*, 127−134.
(36) Vickers, J. W.; Lv, H.; Sumliner, J. M.; Zhu, G.; Luo, Z.; Musaev, D. G.; Geletii, Y. V.; Hill, C. L. *J. Am. Chem. Soc.* **2013**, *135*, 14110−14118.
(37) Junge, H.; Marquet, N.; Kammer, A.; Denurra, S.; Bauer, M.; Wohlrab, S.; Gärtner, F.; Pohl, M.-M.; Spannenberg, A.; Gladiali, S.; Beller, M. *Chem.—Eur. J.* **2012**, *18*, 12749−12758.
(38) Artero, V.; Fontecave, M. *Chem. Soc. Rev.* **2013**, *42*, 2338−2356.
(39) Anxolabéhère-Mallart, E.; Costentin, C.; Fournier, M.; Nowak, S.; Robert, M.; Savéant, J.-M. *J. Am. Chem. Soc.* **2012**, *134*, 6104−6107.
(40) Ghachtouli, S. E.; Fournier, M.; Cherdo, S.; Guillot, R.; Charlot, M.-F.; Anxolabéhère-Mallart, E.; Robert, M.; Aukauloo, A. *J. Phys. Chem. C* **2013**, *117*, 17073−17077.
(41) Ghachtouli, S. E.; Guillot, R.; Brisset, F.; Aukauloo, A. *ChemSusChem* **2013**, *6*, 2226−2230.
(42) Anxolabéhère-Mallart, E.; Costentin, C.; Fournier, M.; Robert, M. *J. Phys. Chem. C* **2014**, *118*, 13377−13381.
(43) Cherdo, S.; Ghachtouli, S. E.; Sircoglou, M.; Brisset, F.; Orio, M.; Aukauloo, A. *Chem. Commun.* **2014**, *50*, 13514−13516.
(44) Fang, M.; Engelhard, M. H.; Zhu, Z.; Helm, M. L.; Roberts, J. A. S. *ACS Catal.* **2013**, *4*, 90−98.
(45) Wang, X.; Goeb, S.; Ji, Z.; Pogulaichenko, N. A.; Castellano, F. N. *Inorg. Chem.* **2011**, *50*, 705−707.
(46) Du, P.; Schneider, J.; Luo, G.; Brennessel, W. W.; Eisenberg, R. *Inorg. Chem.* **2009**, *48*, 4952−4962.
(47) Probst, B.; Rodenberg, A.; Guttentag, M.; Hamm, P.; Alberto, R. *Inorg. Chem.* **2010**, *49*, 6453−6460.
(48) Call, A.; Codolà, Z.; Acuña-Parés, F.; Lloret-Fillol, J. *Chem.—Eur. J.* **2014**, *20*, 6171−6183.
(49) Lv, H.; Guo, W.; Wu, K.; Chen, Z.; Bacsa, J.; Musaev, D. G.; Geletii, Y. V.; Lauinger, S. M.; Lian, T.; Hill, C. L. *J. Am. Chem. Soc.* **2014**, *136*, 14015−14018.
(50) McCrory, C. C.; Uyeda, C.; Peters, J. C. *J. Am. Chem. Soc.* **2012**, *134*, 3164−3170.
(51) Lee, C. H.; Villágran, D.; Cook, T. R.; Peters, J. C.; Nocera, D. G. *ChemSusChem* **2013**, *6*, 1541−1544.
(52) Varma, S.; Castillo, C. E.; Stoll, T.; Fortage, J.; Blackman, A. G.; Molton, F.; Deronzier, A.; Collomb, M. N. *Phys. Chem. Chem. Phys.* **2013**, *15*, 17544−17552.
(53) Ghosh, M.; Weyhermuller, T.; Wieghardt, K. *Dalton Trans.* **2010**, *39*, 1996−2007.
(54) Yamada, Y.; Miyahigashi, T.; Kotani, H.; Ohkubo, K.; Fukuzumi, S. *Energy Environ. Sci.* **2012**, *5*, 6111−6118.
(55) Wang, C.; Cao, S.; Fu, W.-F. *Chem. Commun.* **2013**, *49*, 11251−11253.
(56) Artero, V.; Saveant, J.-M. *Energy Environ. Sci.* **2014**, *7*, 3808−3814.
(57) Felton, G. A. N.; Glass, R. S.; Lichtenberger, D. L.; Evans, D. H. *Inorg. Chem.* **2006**, *45*, 9181−9184.
(58) Karn, J. L.; Busch, D. H. *Nature* **1966**, *211*, 160−162.
(59) Alcock, N. W.; Kingston, R. G.; Moore, P.; Pierpoint, C. *J. Chem. Soc., Dalton Trans.* **1984**, 1937−1943.
(60) Uriarte, R.; Mazanec, T. J.; Tau, K. D.; Meek, D. W. *Inorg. Chem.* **1980**, *19*, 79−85.
(61) Lowry, M. S.; Goldsmith, J. I.; Slinker, J. D.; Rohl, R.; Pascal, R. A., Jr.; Malliaras, G. G.; Bernhard, S. *Chem. Mater.* **2005**, *17*, 5712−5719.
(62) Riker-Nappier, J.; Meek, D. W. *Chem. Commun.* **1974**, 442−443.
(63) Keypour, H.; Stotter, D. A. *Inorg. Chim. Acta* **1979**, *33*, L149−L150.
(64) Vincze, L.; Sándor, F.; Pém, J.; Bosnyák, G. *J. Photoch. Photobio. A: Chem.* **1999**, *120*, 11−14.
(65) Hu, X.; Brunschwig, B. S.; Peters, J. C. *J. Am. Chem. Soc.* **2007**, *129*, 8988−8998.
(66) Costentin, C.; Drouet, S.; Robert, M.; Savéant, J.-M. *Science* **2012**, *338*, 90−94.